e-J. Surf. Sci. Nanotech. Vol. 15 (2017) 55-64 Regular Paper

Visualization of Residual Charges by Atmospheric-Pressure Plasma Jet Irradiation using Dust Figures

Hiroshi Kuwahata,* Takeshi Yamaguchi, and Takaaki Yamaguchi
Department of Electrical and Electronic Engineering, School of Engineering, Tokai University, 4-1-1 Kitakaname, Hiratsuka, Kanagawa 259-1292, Japan
(Received 14 February 2017; Accepted 1 March 2017; Published 29 April 2017)

Dust figures can be used to visualize the distributions of positive and negative charges that remain on the surface of an insulator using two types of charged powder; one is attached to the insulator and positive charges, and the other is attached to negative charges. In this study, dust figures were used to visualize the spreading pattern of an atmospheric-pressure plasma jet when an insulator was irradiated with the plasma jet in air. Observation using a high-speed camera indicates that streamers existed in the plasma and served as a source of both positive and negative charges. An ebonite plate was used as an insulator. White rosin powder and red lead (colored orange) powder were used to obtain positive and negative charge diagrams, respectively. When the ebonite plate was irradiated with an atmospheric-pressure argon (Ar) plasma jet in air, a disc- or ring-shaped dust figure was formed because of the residual positive and negative charges. The shape and size of the dust figure depended on the spreading pattern of the plasma jet on the ebonite plate. The dependence of the dust figure formed by both charges on the irradiation time (1–60 s) and distance (2–40 mm) of the plasma, the applied voltage (4–10 kV), and the Ar gas flow rate (5 or 10 L/min)was determined. [DOI: 10.1380/ejssnt.2017.55]

Keywords: Plasma processing; Surface electronic phenomena; Insulating surfaces; Dust figure; atmospheric-pressure plasma

I. INTRODUCTION

Lichtenberg figures are branching, tree-like patterns that are created by the passage of high-voltage electrical discharges along the surface of, or through, electrically insulating materials. The first Lichtenberg figures were actually two-dimensional "dust figures" that formed when airborne dust settled on the surface of electrically charged plates of resin as described by Lichtenberg in 1777 [1]. In his studies, he used various insulating materials including resin, glass, and ebonite (hard rubber). He then sprinkled mixtures of finely powdered sulfur and red lead onto the charged surfaces. He found that powdered sulfur (which became negatively charged through friction inside its container) was more strongly attracted to the positively charged regions. Similarly, frictionally charged particles of red lead acquired a positive charge and were attracted to negatively charged regions. In 1921, Toepler placed a needle and plate electrodes in a dark box, inserted a photographic plate between the electrodes while the photosensitive surface was facing the needle electrode, and applied an impulse voltage to the electrodes [2]. He observed figures on the photosensitive surface and reported that the shape and size of the figures depended on the magnitude and polarity of the impulse voltage. Since then, such figures have been used to analyze discharge phenomena [3–10]. Lichtenberg figures now mostly refer to the figures obtained using photosensitive materials.

Dust figures are obtained by sprinkling charged powders on the surface of an insulator after applying a discharge over the insulator. This occurs because the charged powders are attached to the sites where bipolar charges are present because of the electrostatic force [11]. In 1928, Toriyama first reported his research on dust figures using charged powders and an ebonite plate as an insulator [12]. He clarified that dust figures have sufficient reproducibility for use in the measurement of voltage and the evaluation of polarity. He also revealed that polarity can be easily evaluated from the color of charged powders, i.e., the development of images in a dark room is not required, and insulators can be recycled many times. Thus, he reported that dust figures can be widely used to analyze discharge phenomena, similarly to the Lichtenberg figures obtained using photographic plates [13–17]. Regarding dust figures, positive and negative charge diagrams are obtained because positive ions and electrons remain on the surface of an ebonite plate [15]. In 1928, Toriyama experimented with two types of charged mixed powder: (1) a mixed powder of red lead (colored orange) and yellow sulfur and (2) a mixed powder of white lead acetate and yellow sulfur [13]. From 1929, he used a mixed powder of red lead and white rosin to facilitate color discrimination [15, 17]. In 1973, Murooka et al. used glass plates, on one face of which a very thin silicon film was sprayed as an insulator, mixtures of red-colored lead oxide and yellow-white sulfur as a charged powder [18]. In 1979, Ando et al. used a mixed powder of red lead and yellow sulfur [19]. In 1994, Manabe et al. used an acrylic plate as an insulator and white zinc oxide as a charged powder [20].

In our previous studies, various materials, such as insulating quartz glass [21], semiconducting silicon [22], metallic aluminum [23], bacteria [24], organic phospholipids [25], and water that contains organic compounds [26] were irradiated by an atmospheric-pressure Ar plasma jet $\sim$ 20 mm long with a maximum diameter of 6 mm ejected into air. The changes in these materials upon plasma jet irradiation in air were examined. When materials with a low electric conductivity, such as insulators and semiconductors, were irradiated with an Ar plasma jet, the plasma that reached the materials laterally spread in a disc shape. In contrast, when materials with a high electric conductivity, such as metals and water containing impurities, were irradiated with an Ar plasma jet, the plasma that reached the materials did not spread laterally. Thus, we found that the spreading pattern of the plasma depended on the electrical conductivity of the

* Corresponding author: kuwahata@tokai-u.jp

 © 2017 The Surface Science Society of Japan (http://www.sssj.org/ejssnt)

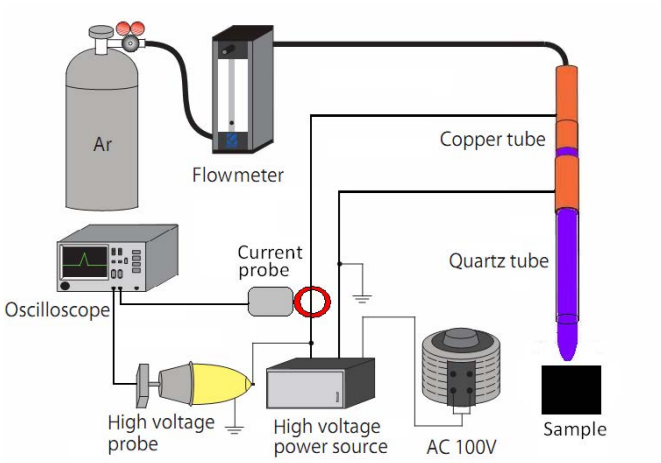

FIG. 1. Schematic of experimental setup [28].

FIG. 2. Photograph of ebonite plate.

FIG. 3. Photographs of charged powders: (a) rosin powder, which adheres to the residual positive charges, and (b) red lead powder, which adheres to the residual negative charges.

irradiated targets. In addition, we examined how the positively charged Ar ions and negatively charged electrons in the plasma were distributed on the irradiation targets. In these studies, we focused on the dust figures that can be used to discriminate positive and negative charges from the color of the charged powders used. In previous studies using dust figures, a mixture of two types of charged powder was used. In this study, we used two types of charged powder separately because the positively charged Ar ions and negatively charged electrons were simultaneously present in the Ar plasma. The dust figures were used to visualize how an atmospheric-pressure Ar plasma jet behaved on the surface of insulators that were irradiated with the plasma jet in air.

In this study, we used an ebonite plate, similarly to that used in the study of Toriyama [15, 17], white rosin powder, which was attracted to positive charges, and red lead powder, which was attracted to negative charges. The ebonite plate was irradiated with an atmospheric-pressure Ar plasma jet, and the distributions of the positive and negative charges remaining on the ebonite plate were visualized. The presence of the positive and negative charges on the plate indicated that Ar ions and electrons reached the plate. In this paper, we report the dependence of the dust figures formed by the residual positive and negative charges on the irradiation time and distance of the plasma, the applied voltage, and the Ar gas flow rate. To the best of our knowledge, there have been no reports on the analysis of atmospheric-pressure plasma using dust figures.

II. EXPERIMENTAL

Figure 1 shows a schematic of the experimental setup used in this study. In the unit used to generate a plasma jet, a copper tube (inner diameter, 4 mm; outer diameter, 6 mm) as the discharge electrode was inserted into a dielectric quartz tube (length, 50 mm; inner diameter, 6 mm; outer diameter, 8 mm), around which a copper foil (thickness, 0.05 mm; width, 10 mm) was wrapped as the ground electrode [27]. A high AC voltage was applied to induce dielectric barrier discharge inside the quartz tube between the electrodes and to convert the Ar gas to plasma, which was then ejected into the air in the form of a jet. A high-voltage power supply (LHV-10AC, Logy Electric Co., Ltd.) was used to generate the Ar plasma jet (frequency, 10 kHz; applied voltage, 4–10 kV; Ar gas flow rate, 5 or 10 L/min).An ebonite plate was irradiated with the Ar plasma jet for 1–60 s. The distance from the end of the quartz tube to the ebonite plate (irradiation distance) was in the range of 2–40 mm. The voltage and current were measured using a high-voltage probe (P6015A, Tektronix, Inc.) and a current probe (A621, Tektronix, Inc.), respectively, which were both connected to a digital oscilloscope (TDS1001B, Tektronix, Inc.). The gas flow rate was adjusted using a gas flowmeter (RK-1250, Kofloc Kyoto, Kojima Instruments Inc.). A high-speed camera (FASTCAM SA-Z, Photron Ltd.) was used to take photographs at 100,000 fps.

Figure 2 shows a photograph of the ebonite plate ($\sim 50 \times 50 \times 5\text{mm}^3$). Ebonite is a brown-black glossy hard rubber fabricated by heating a mixture of natural rubber and sulfur; it is used for electrical insulation and in fountain pens. The surface of the ebonite plate was rinsed with ethanol and dried using a dryer before plasma jet irradiation.

Figure 3 shows photographs of the charged powders. Figure 3(a) shows white rosin ($C_{20}H_{30}O_2$) powder, which is attracted to the residual positive charges. This is a natural resin mainly composed of the rosin acid contained in pine resin, the sap of pine trees, which is used as a non-slip material. In this study, rosin was purchased from Kanto

FIG. 4. Schematic dust figures on the ebonite plate. (a) Residual positive charges and (b) residual negative charges.

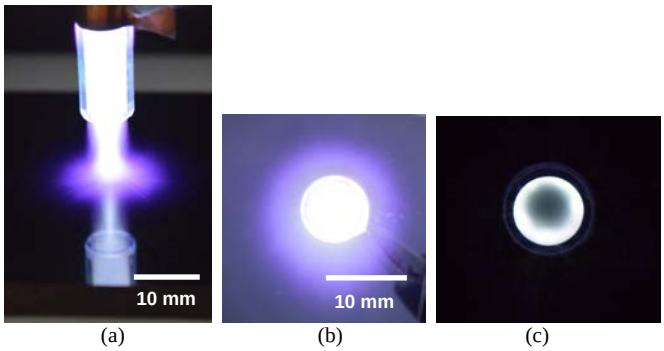

FIG. 5. Ejection of plasma jet (applied voltage, 10 kV; gas flow rate, 10 L/min; irradiation distance, 10 mm): (a) irradiation of ebonite plate, (b) photograph taken above quartz plate at a small aperture, and (c) photograph taken above quartz plate at a large aperture.

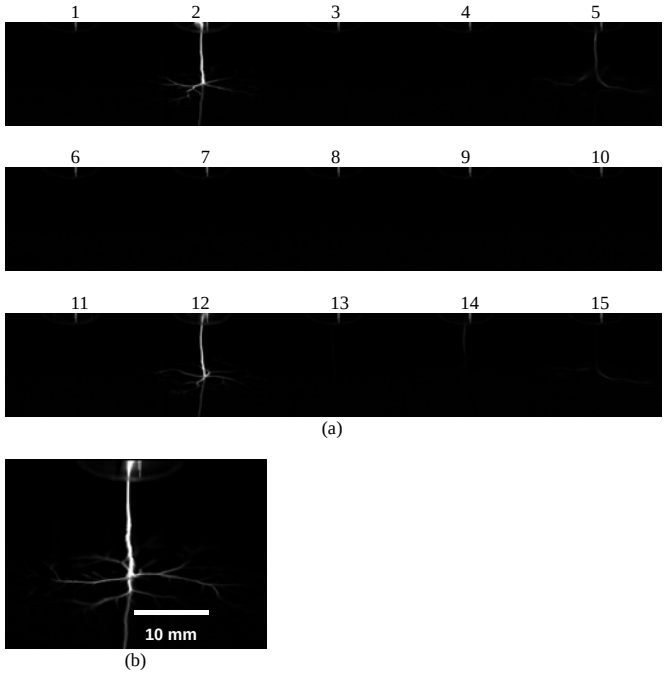

FIG. 6. High-speed camera images of plasma jet ejected toward an ebonite plate (applied voltage, 10 kV; gas flow rate, 10 L/min; irradiation distance, 10 mm): (a) 15 consecutive frames and (b) enlarged image of second frame.

Chemical Co., Inc., and finely ground using a mortar. Figure 3(b) shows red lead (Pb_3O_4) powder, colored orange, which is attracted to the residual negative charges. This is an inorganic compound consisting of lead and oxygen and is used for red pigments. In this study, red lead was purchased from Wako Pure Chemical Industries, Ltd. After plasma jet irradiation, rosin or red lead powder was sprinkled on the ebonite plate, and excess powder was removed using a blower.

Figure 4 shows schematic dust figures on the ebonite plate. When positive charges remain on the surface of the ebonite plate, white rosin powder adheres to the plate, as shown in Fig. 4(a). When negative charges remain, red lead powder (in orange) adheres to the plate, as shown in Fig. 4(b).

III. RESULTS AND DISCUSSION

Figure 5 illustrates the ejection of a plasma jet. Figure 5(a) shows a photograph of a plasma jet ejected toward an ebonite plate. Figures 5(b) and 5(c) show photographs of a plasma jet taken above a quartz plate at small and large apertures, respectively. As shown in Fig. 5(a), the plasma ejected from the end of the quartz tube reached the ebonite plate and laterally spread in a disc shape with a diameter of $\sim$ 20 mm. As shown in Fig. 5(b), the plasma that reached the quartz plate laterally spread in a disc shape with a diameter of $\sim$ 20 mm. In Fig. 5(c), the center of the quartz tube was dark, whereas the area near the inner wall of the quartz tube was bright. This result indicates that the plasma was distributed nonuniformly and concentrated along the inner wall of the quartz tube.

Figure 6 shows high-speed camera images of a plasma jet ejected towards an ebonite plate. Figure 6 (a) shows 15 consecutive frames obtained at intervals of 0.01 ms. The streamers reached the ebonite plate in the second frame and also in the 12th frame. The interval between the two frames (0.1 ms) was equal to the period of the AC with a frequency of 10 kHz from the power source. This result indicates that the streamer discharge occurred at a rate of 10,000 times per second in the Ar plasma jet [23]. Weak streamers were also observed in the fifth and 15th frames. These are considered to be back discharge or after-discharge, in which the charges stored on the surface of the ebonite plate are reversibly discharged. The mechanism of back discharge is as follows. When a primary discharge (a discharge that occurs while the applied voltage is increasing) occurs, the charges stored on the insulating plate generate an electric field opposite to the applied voltage. When the application of voltage stops, a secondary discharge is induced [8, 29]. Our results indicate that a back discharge occurred 0.03 ms after the discharge. Figure 6 (b) shows an enlarged image of the second frame. A streamer reached the ebonite plate and laterally spread in a tree shape on the plate. The diameter of the streamer was $\sim$ 20 mm. The plasma jet ejected toward an ebonite plate in Fig. 5(a) is considered to be the result of overlapping multiple streamers. In the streamers, Ar atoms in Ar gas are continuously ionized, and Ar ions and electrons coexist. Therefore, both positive and negative charges are present in the streamers.

Figure 7 shows the dependence of the dust figure on the irradiation time of the plasma. Figures 7(a)–7(f) show the dust figures formed by the positive charges remaining on the ebonite plate as a result of sprinkling rosin powder, whereas Figs. 7(g)–7(l) show those formed by the negative charges remaining on the ebonite plate as a result of

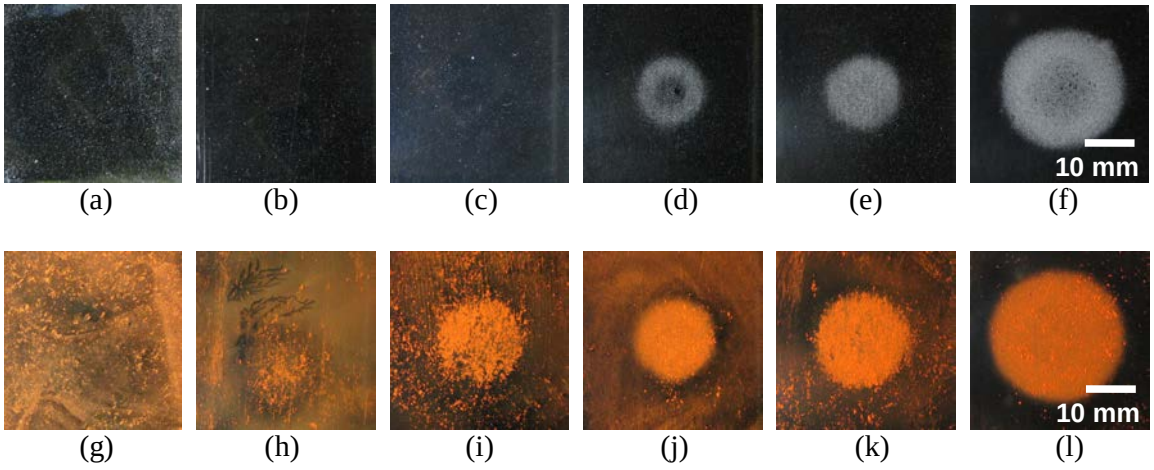

FIG. 7. Dependence of dust figure on irradiation time of plasma (applied voltage, 10 kV; gas flow rate, 10 L/min; irradiation distance, 10 mm): (upper figures) positive charge diagrams (rosin powder), (a) before irradiation, (b) 1 s, (c) 5 s, (d) 10 s, (e) 30 s, and (f) 60 s; (lower figures) negative charge diagrams(red lead powder), (g) before irradiation, (h) 1 s, (i) 5 s, (j) 10 s, (k) 30 s, and (l) 60 s.

sprinkling red lead powder. In the case of the positive charges, rosin did not adhere to the plate for irradiation times of ≤ 5 s but did adhere to the plate for irradiation times of ≥ 10 s. The region in which the rosin adhered was disc-shaped. The diameter of the disc increased with increasing irradiation time; it was ~ 19 mm for an irradiation time of 10 s [Fig. 7(d)], ~ 20 mm for an irradiation time of 30 s [Fig. 7(e)], and ~ 28 mm for an irradiation time of 60 s [Fig. 7(f)]. In the case of the negative charges, red lead adhered to the plate for irradiation times of ≥ 1 s. The region in which the red lead adhered was also disc-shaped. The diameter of the disc increased with increasing irradiation time; it was ~ 15 mm for an irradiation time of 1 s [Fig. 7(h)], ~ 23 mm for an irradiation time of 5 s [Fig. 7(i)], ~ 23 mm for an irradiation time of 10 s [Fig. 7(j)], ~ 26 mm for an irradiation time of 30 s [Fig. 7(k)], and ~ 32 mm for an irradiation time of 60 s [Fig. 7(l)]. The adhesion of both rosin and red lead indicates that both positive and negative charges remained on the ebonite plate irradiated with a plasma. The times required until the rosin and red lead started adhering and the diameters of the discs in which they adhered were slightly different. This is thought to be due to the difference in adhesiveness of the two charged powders, which depends on, for example, the size of the particles. However, there was thought to be no difference in the amount of residual charges or the spreading pattern of the charges. Because the sizes of the dust figures formed by the positive and negative charges were almost the same, the distribution areas of the two charges in the plasma were confirmed to be the same. The reason why the diameter of the disc increased with the irradiation time of the plasma may be due to the fact that the amount of charges remaining on the ebonite plate increased, which caused a repulsive force to act between the charges, resulting in the lateral spread of the charged particles.

Figure 8 shows the dependence of the diameter of the disc-shaped region of powder on the ebonite plate on the irradiation time of the plasma. The diameter of the disc

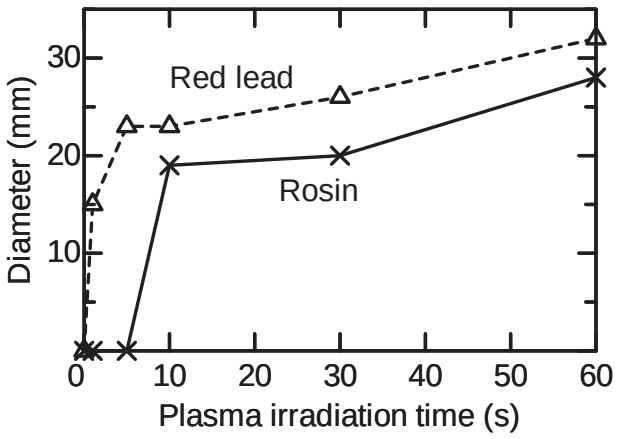

FIG. 8. Dependence of the diameter of the disc on the ebonite plate on the irradiation time of the plasma.

increased with increasing irradiation time for both rosin and red lead powders.

Figure 9 shows photographs of a plasma jet ejected toward an ebonite plate and the dust figures on the ebonite plate for different irradiation distances. For irradiation distances of ≥ 30 mm [Figs. 9(a) and 9(b)], the plasma ejected from the quartz tube does not appear to reach the ebonite plate. For irradiation distances of ≤ 20 mm [Figs. 9(c)–9(e)], the plasma appears to have reached the ebonite plate and laterally spreads in a disc shape. The diameter of the disc was ~ 7 mm for an irradiation distance of 20 mm [Fig. 9(c)], ~ 19 mm for an irradiation distance of 10 mm [Fig. 9(d)], and ~ 24 mm for an irradiation distance of 2 mm [Fig. 9(e)]. The spread of the plasma on the ebonite plate increased as the irradiation distance decreased. Figures 9(f)–9(j) show the dust figures formed by the residual positive charges as a result of sprinkling rosin powder, whereas Figs. 9(k)–9(o) show those formed by the residual negative charges as a

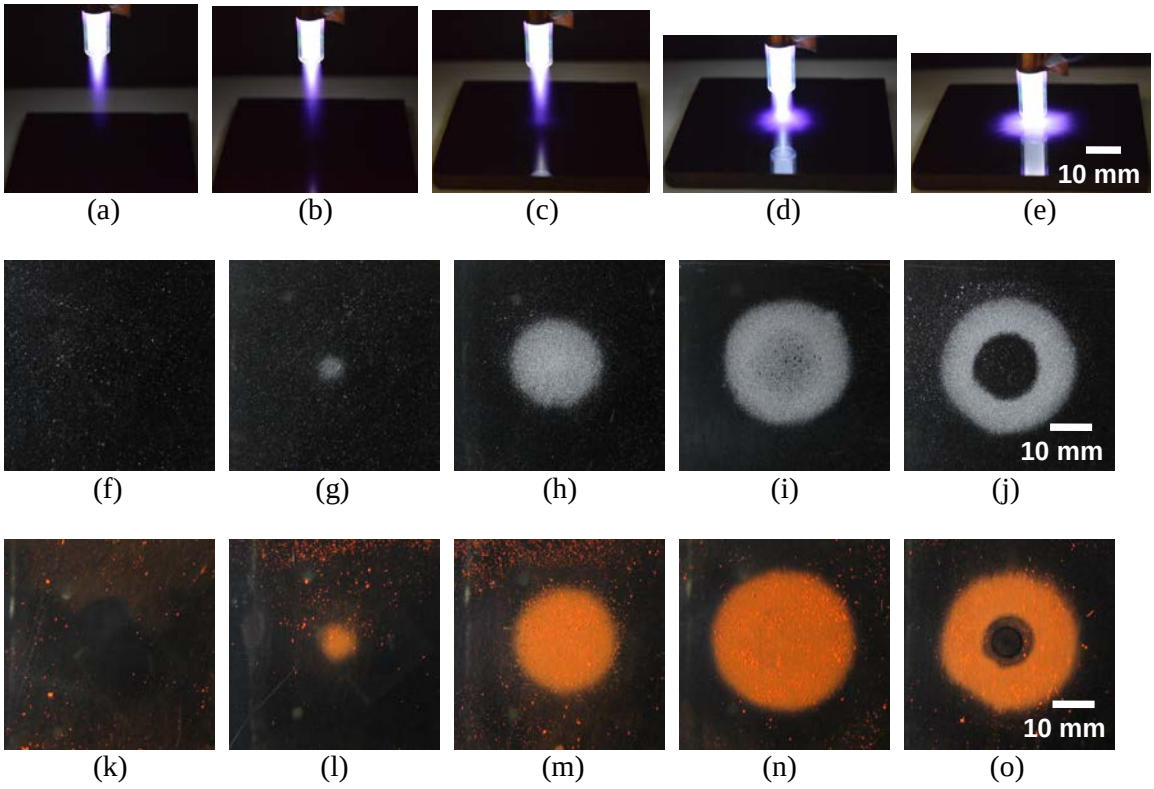

FIG. 9. Plasma jet ejected toward an ebonite plate for different irradiation distances (applied voltage, 10 kV; gas flow rate, 10 L/min; irradiation time, 60 s): (a) 40 mm, (b) 30 mm, (c) 20 mm, (d) 10 mm, and (e) 2 mm. Dust figures on ebonite plate: (upper figures) positive charge diagrams (rosin powder), (f) 40 mm, (g) 30 mm, (h) 20 mm, (i) 10 mm, and (j) 2 mm; (lower figures) negative charge diagrams (red lead powder), (k) 40 mm, (l) 30 mm, (m) 20 mm, (n) 10 mm, and (o) 2 mm.

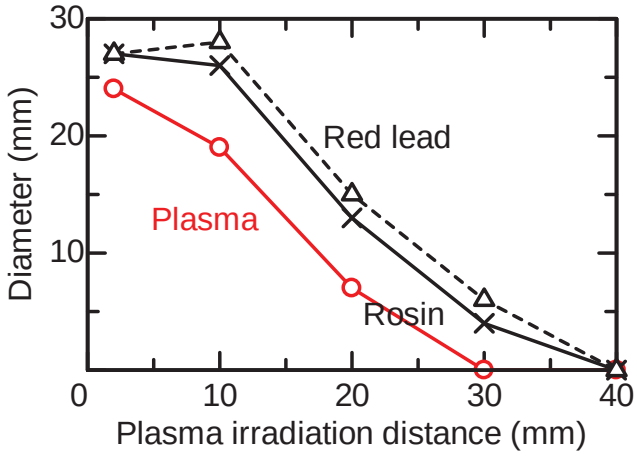

FIG. 10. Dependence of the diameter of the disc (the spread of the plasma) on the ebonite plate on the irradiation distance of the plasma.

result of sprinkling red lead powder. In the case of positive charges, the rosin did not adhere to the ebonite plate for an irradiation distance of 40 mm [Fig. 9(f)]. However, the rosin adhered to the plate in a disc shape for irradiation distances of 10–30 mm [Figs. 9(g)–9(i)]. The diameter of the disc increased as the irradiation distance decreased; it was ∼ 4 mm for an irradiation distance of 30 mm [Fig. 9(g)], ∼ 13 mm for an irradiation distance of 20 mm [Fig. 9(h)], and ∼ 26 mm for an irradiation distance of 10 mm [Fig. 9(i)]. For an irradiation distance of 2 mm [Fig. 9(j)], the rosin adhered to the plate in a ring shape with an inner diameter of ∼ 15 mm and an outer diameter of ∼ 27 mm. In the case of negative charges, the red lead did not adhere to the ebonite plate for an irradiation distance of 40 mm [Fig. 9(k)]. However, it adhered to the plate in a disc shape for irradiation distances of 10–30 mm [Figs. 9(l)–9(n)]. The diameter of the disc increased as the irradiation distance decreased; it was ∼ 6 mm for an irradiation distance of 30 mm [Fig. 9(l)], ∼ 15 mm for an irradiation distance of 20 mm [Fig. 9(m)], and ∼ 28 mm for an irradiation distance of 10 mm [Fig. 9(n)]. For an irradiation distance of 2 mm [Fig. 9(o)], the red lead adhered to the plate in a ring shape with an inner diameter of ∼ 12 mm and an outer diameter of ∼ 27 mm. The dust figures formed by the negative charges (using red lead) were slightly larger than those formed by the positive charges (using rosin). This difference may be due to the difference in the adhesiveness of the two powders, as discussed for Fig. 7. The spreading patterns of the positive and negative charges on the ebonite plate with respect to the irradiation distance are thought to be the same. Comparing the spreading pattern of the plasma jet on the ebonite plate and the size and shape of the dust figures, it can be seen that the rosin and red lead adhered to the region irradiated with a plasma jet. Therefore, it was confirmed that the plasma did not reach the ebonite plate for an irradiation distance of 40 mm because neither

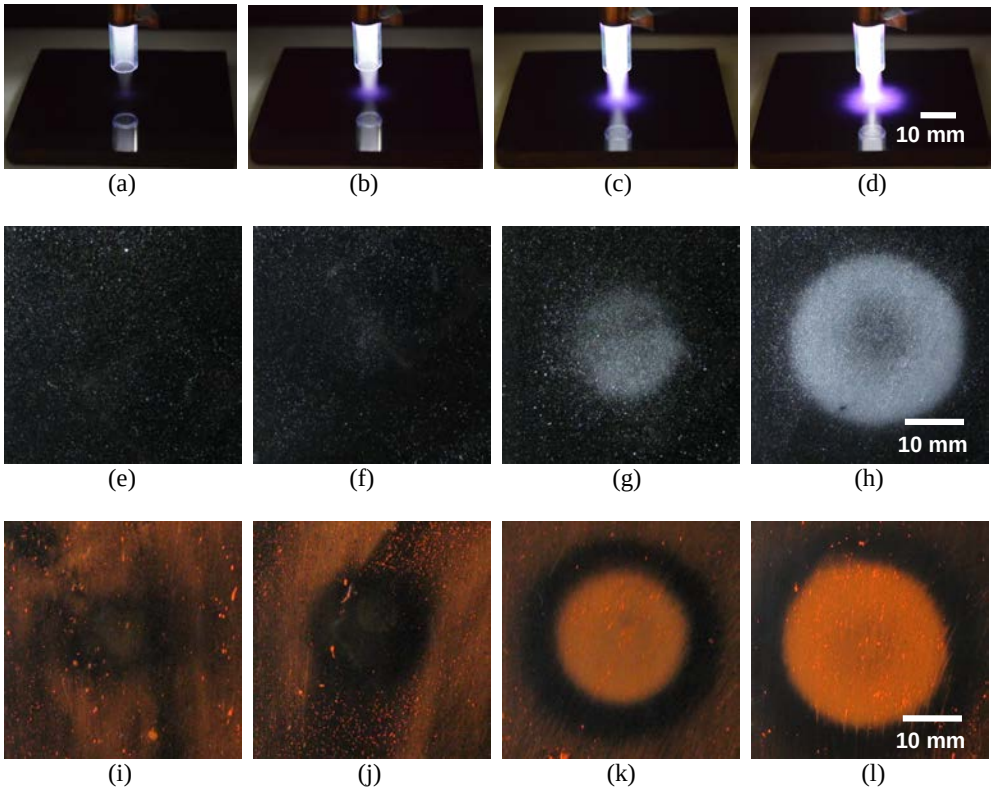

FIG. 11. Plasma jet ejected toward an ebonite plate for an irradiation distance of 10 mm and different applied voltages (gas flow rate, 10 L/min; irradiation time, 60 s): (a) 4 kV, (b) 6 kV, (c) 8 kV, and (d) 10 kV. Dust figures on ebonite plate: (upper figures) positive charge diagrams (rosin powder), (e) 4 kV, (f) 6 kV, (g) 8 kV, and (h) 10 kV; (lower figures) negative charge diagrams (red lead powder), (i) 4 kV, (j) 6 kV, (k) 8 kV, and (l) 10 kV.

rosin nor red lead adhered to the plate. For an irradiation distance of 30 mm, the plasma did not appear to have reached the ebonite plate but the rosin and red lead started adhering to the plate, indicating that the charged particles reached the ebonite plate. When the irradiation distance further decreased, the plasma that reached the plate laterally spread in a disc shape. For an irradiation distance of 2 mm [Figs. 9(j) and 9(o)], the rosin and red lead did not adhere to the center of the plate. This indicates that the streamers were nonuniformly distributed inside the quartz tube and flowed along the inner wall of the quartz tube before being ejected into air. Then, the streamers reached the ebonite plate and laterally spread in a disc shape. That is, fewer streamers are present at the center than along the inner wall of the quartz tube, resulting in a reduced amount of charged powder adhering to the center of the plate. The fact that the diameter of the disc increased with decreasing irradiation distance indicates that the streamers that reached the ebonite plate laterally spread further for shorter irradiation distances.

Figure 10 shows the dependence of the diameter of the disc (i.e., the spread of the plasma on the ebonite plate) on the irradiation distance of the plasma. As the irradiation distance increased, the spread of the plasma decreased and the diameter of the disc accordingly decreased.

Figure 11 shows photographs of a plasma jet ejected to the ebonite plate and the dust figures on the plate for an irradiation distance of 10 mm and different applied voltages. For an applied voltage of 4 kV [Fig. 11(a)], the plasma appeared to be ejected outside the quartz tube. However, for applied voltages of $\geq$ 6 kV [Figs. 11(b)–11(d)], the plasma appeared to be ejected outside the quartz tube, reach the ebonite plate, and laterally spread in a disc shape on the ebonite plate. The diameter of the disc increased with the applied voltage; it was $\sim$ 12 mm for an applied voltage of 6 kV, $\sim$ 15 mm for an applied voltage of 8 kV, and $\sim$ 20 mm for an applied voltage of

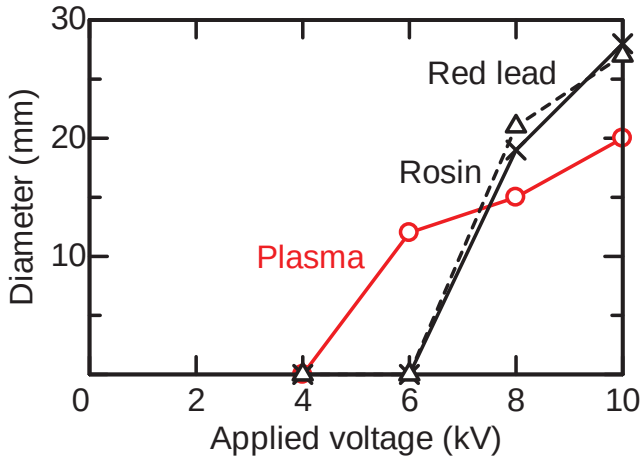

FIG. 12. Dependence of the diameter of the disc (the spread of the plasma) on the ebonite plate on the applied voltage (irradiation distance of 10 mm).

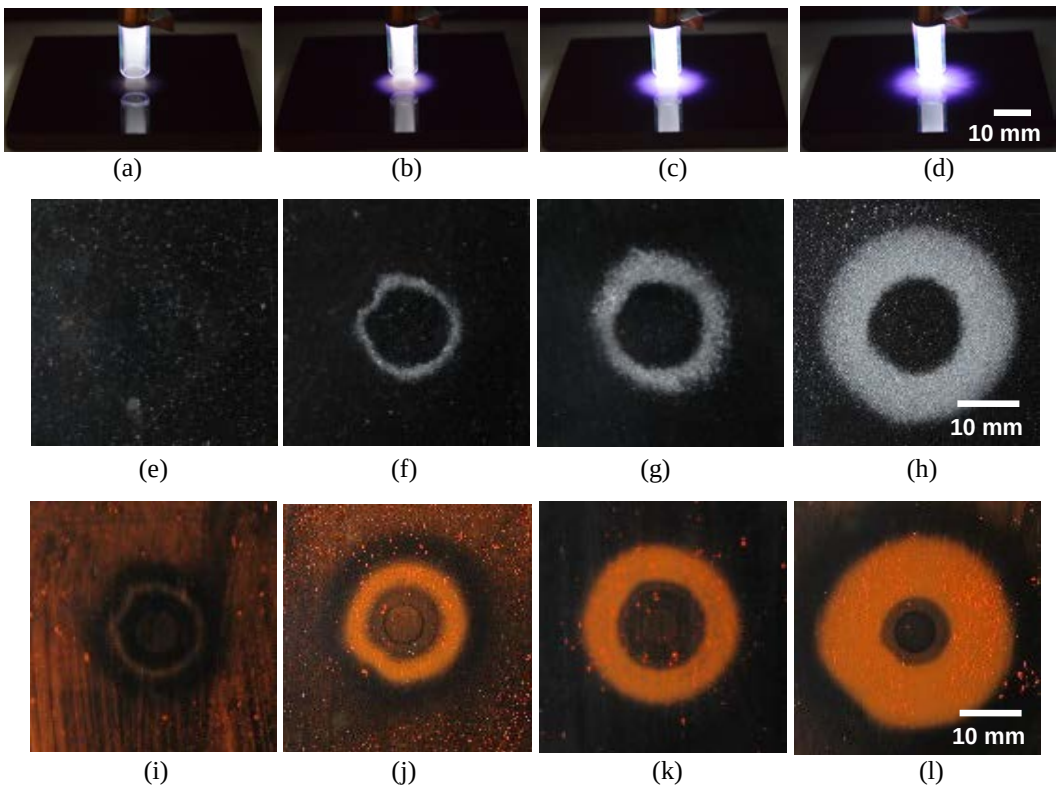

FIG. 13. Plasma jet ejected toward an ebonite plate for an irradiation distance of 2 mm and different applied voltages (gas flow rate, 10 L/min; irradiation time, 60 s): (a) 4 kV, (b) 6 kV, (c) 8 kV, and (d) 10 kV. Dust figures on ebonite plate: (upper figures) positive charge diagrams (rosin powder), (e) 4 kV, (f) 6 kV, (g) 8 kV, and (h) 10 kV; (lower figures) negative charge diagrams (red lead powder), (i) 4 kV, (j) 6 kV, (k) 8 kV, and (l) 10 kV.

10 kV. Figures 11(e)–11(h) show the dust figures formed by the residual positive charges as a result of sprinkling rosin powder, and Figs. 11(i)–11(l) show those formed by the residual negative charges as a result of sprinkling red lead powder. In the case of positive charges, the rosin did not adhere to the ebonite plate for applied voltages of $\leq$ 6 kV but adhered to the plate in a disc shape for applied voltages of $\geq$ 8 kV. These results indicate that there was little quantity of electric charges in the plasma for applied voltages of $\leq$ 6 kV. The diameter of the disc increased with the applied voltage; it was $\sim$ 19 mm for an applied voltage of 8 kV [Fig. 11(g)] and $\sim$ 28 mm for an applied voltage of 10 kV [Fig. 11(h)]. Also in the case of negative charges, the red lead did not adhere to the ebonite plate for applied voltages of $\leq$ 6 kV but adhered to the plate in a disc shape for applied voltages of $\geq$ 8 kV. These results indicate that there was little quantity of electric charges in the plasma for applied voltages of $\leq$ 6 kV. The diameter of the disc increased with the applied voltage; it was $\sim$ 21 mm for an applied voltage of 8 kV [Fig. 11(k)] and $\sim$ 27 mm for an applied voltage of 10 kV [Fig. 11(l)]. The fact that the diameter of the disc increased with the applied voltage indicates that the streamers that reached the ebonite plate laterally spread further for higher applied voltages.

Toepler reported that the diameter of a Lichtenberg figure increased with the applied voltage when an impulse voltage was applied between a needle and plate electrodes [2]. Our results were similar to his results.

Figure 12 shows the dependence of the diameter of the disc (the spread of the plasma on the ebonite plate) on the applied voltage at an irradiation distance of 10 mm. As the applied voltage increased, the spread of the plasma increased and the diameter of the disc accordingly increased.

Figure 13 shows photographs of a plasma jet ejected toward an ebonite plate and the dust figures on the ebonite plate for an irradiation distance of 2 mm and different applied voltages. For applied voltages of $\geq$ 4 kV [Figs. 13(a)–13(d)], the plasma, which appeared to be ejected outside the quartz tube, reached the ebonite plate, and laterally spread in a disc shape on the ebonite plate. The diameter of the disc increased with the applied voltage; it was $\sim$ 18 mm for an applied voltage of 6 kV, $\sim$ 22 mm for an applied voltage of 8 kV, and $\sim$ 27 mm for an applied voltage of 10 kV. Figures 13(e)–13(h) show the dust figures formed by the residual positive charges as a result of sprinkling rosin powder, and Figs. 13(i)–13(l) show those formed by the residual negative charges as a result of sprinkling red lead powder. In the case of positive charges, the rosin did not adhere to the ebonite plate for an applied voltage of 4 kV but adhered to the plate in a ring shape for applied voltages of $\geq$ 6 kV. These results indicate that there was little quantity of electric charges in the plasma for applied voltages of $\leq$ 4 kV. The inner and outer diameters of the ring were $\sim$ 13 and $\sim$ 15 mm for an applied voltage of 6 kV [Fig. 13(f)], $\sim$ 14 and $\sim$ 18 mm for an applied voltage of 8 kV [Fig. 13(g)], and $\sim$ 14

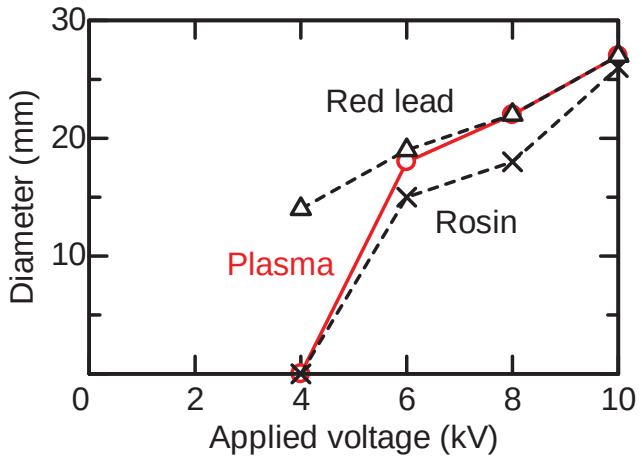

FIG. 14. Dependence of the diameter of the disc (the spread of the plasma) on the ebonite plate on the applied voltage (irradiation distance of 2 mm).

and ∼ 26 mm for an applied voltage of 10 kV [Fig. 13(h)], respectively. With increasing applied voltage, the outer diameter increased but the inner diameter decreased. In the case of negative charges, the red lead adhered to the plate in a ring shape for applied voltages of ≥ 4 kV. The inner and outer diameters of the ring were ∼ 12 and ∼ 14 mm for an applied voltage of 4 kV [Fig. 13(i)], ∼ 12 and ∼ 19 mm for an applied voltage of 6 kV [Fig. 13(j)], ∼ 13 and ∼ 22 mm for an applied voltage of 8 kV [Fig. 13(k)], and ∼ 11 and ∼ 27 mm for an applied voltage of 10 kV [Fig. 13(l)], respectively. With increasing applied voltage, the outer diameter increased but the inner diameter decreased. The fact that the outer diameter of the ring increased with the applied voltage indicates that the streamers that reached the ebonite plate laterally spread further for higher applied voltages.

Figure 14 shows the dependence of the diameter of the disc (the spread of the plasma on the ebonite plate) on the applied voltage at an irradiation distance of 2 mm. As the applied voltage increased, the spread of the plasma increased and the diameter of the disc accordingly increased.

Figure 15 shows photographs of a plasma jet ejected toward an ebonite plate and the dust figures on the ebonite plate for different Ar gas flow rates. For an Ar gas flow rate of ≥ 5 L/min [Figs. 15(a) and 15(b)], the plasma, which appeared to be ejected outside the quartz tube, reached the ebonite plate, and laterally spread in a disc shape on the ebonite plate. The diameter of the disc increased with the Ar gas flow rate; it was ∼ 13 mm for an Ar gas flow rate of 5 L/min [Fig. 15(a)] and ∼ 22 mm for an Ar gas flow rate of 10 L/min [Fig. 15(b)]. Figures 15(c) and 15(d) show the dust figures formed by the residual positive charges as a result of sprinkling rosin powder, and Figs. 15(e) and 15(f) show those formed by the residual negative charges as a result of sprinkling red lead powder. In the cases of both charges, the rosin and red lead adhered to the ebonite plate for Ar gas flow rates of ≥ 5 L/min. The diameter of the disc in the case of using rosin increased with the Ar gas flow rate; it was ∼ 16 mm for an Ar gas flow rate of 5 L/min [Fig. 15(c)] and ∼ 28 mm for an Ar gas flow rate of 10 L/min [Fig. 15(d)].

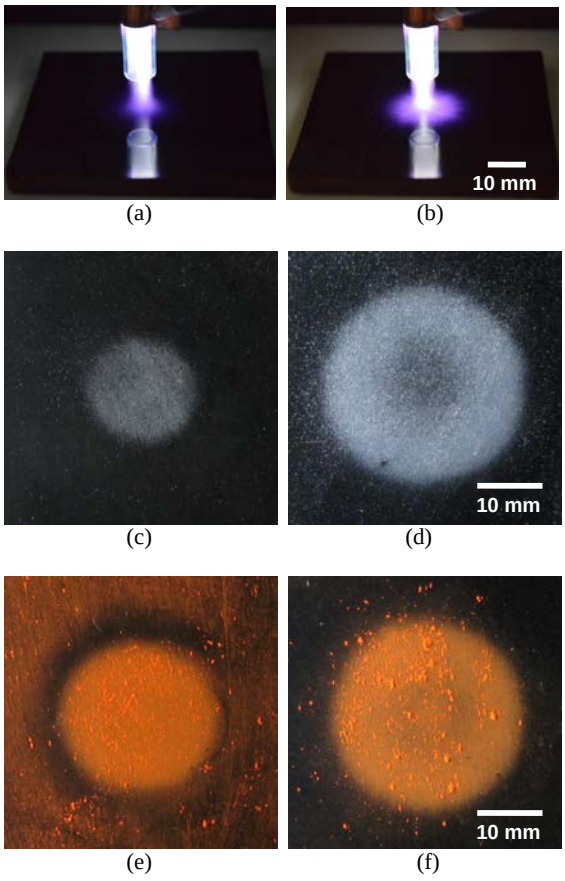

FIG. 15. Plasma jet ejected toward an ebonite plate at different gas flow rates (applied voltage, 10 kV; irradiation distance, 10 mm; irradiation time, 60 s): (a) 5 L/min and (b) 10 L/min. Dust figures on ebonite plate: (upper figures) positive charge diagrams (rosin powder), (c) 5 L/min and (d) 10 L/min; (lower figures) negative charge diagrams (red lead powder), (e) 5 L/min and (f) 10 L/min.

The diameter of the disc in the case of using red lead also increased with the Ar gas flow rate; it was ∼ 23 mm for an Ar gas flow rate of 5 L/min [Fig. 15(e)] and ∼ 27 mm for an Ar gas flow rate of 10 L/min [Fig. 15(f)].The fact that the diameter of the disc increased with the Ar gas flow rate indicates that the streamers that reached the ebonite plate laterally spread further for higher Ar gas flow rates.

Figure 16 shows the dependence of the diameter of the disc (the spread of the plasma on the ebonite plate) on the gas flow rate. As the gas flow rate increased, the spread of the plasma increased and the diameter of the disc accordingly increased.

Figure 17 shows the difference in the spreading pattern of the streamers on the insulating material for different irradiation distances, obtained from dust figures. The streamers in the plasma are nonuniformly distributed in the quartz tube but are concentrated in the vicinity of its inner wall. When the insulating material is irradiated with a plasma jet, the streamers reach the insulating material and spread laterally in the case of long irradiation distances [Fig. 17(a)]. In contrast, for short irradiation distances [Fig. 17(b)], the streamers flow outward along

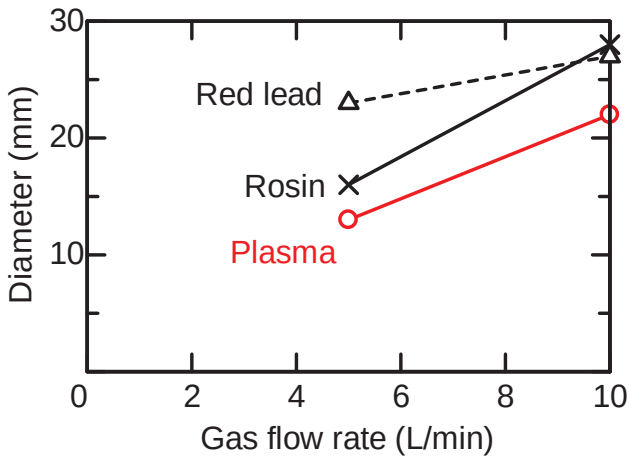

FIG. 16. Dependence of the diameter of the disc (the spread of the plasma) on the ebonite plate on the gas flow rate.

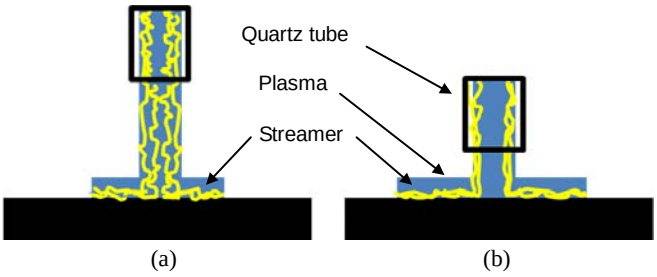

FIG. 17. Difference in spreading pattern of streamers on the insulating material obtained from dust figures. (a) Long irradiation distance and (b) short irradiation distance.

the inner wall of the quartz tube, reach the insulating material, and then spread laterally. Therefore, the center of the plasma-irradiated spot is not reached by the streamers, meaning that no charges remain and charged particles do not adhere to this area.

IV. CONCLUSION

Dust figures were used to visualize the spreading pattern of an atmospheric-pressure Ar plasma jet on an insulator irradiated by the jet in air. Observation using a high-speed camera revealed that streamers existed in the plasma and served as a source of both positive and negative charges. To obtain dust figures, an ebonite plate was used as an insulator, and rosin powder and red lead powder were used to visualize the distribution of the positive and negative charges remaining on the ebonite plate, respectively. After the ebonite plate was irradiated with an Ar plasma jet, dust figures formed by both charges were observed, confirming that positive and negative charges were contained in the Ar plasma jet. It was also confirmed that the distribution areas of the positive and negative charges in the plasma were the same because the sizes of the dust figures formed by the positive and negative charges were almost the same.

The dependence of the dust figures formed by the residual positive and negative charges on the irradiation time (1–60 s) and distance (2–40 mm) of the plasma, the applied voltage (4–10 kV), and the Ar gas flow rate (5 or 10 L/min)was determined as follows.

1) Dependence on irradiation time of plasma: The dust figures formed by both charges on the ebonite plate irradiated with an atmospheric-pressure Ar plasma jet for an irradiation distance of 10 mm were disc-shaped. The diameter of the disc increased with the irradiation time.

2) Dependence on irradiation distance of plasma: No dust figure was observed for an irradiation distance of 40 mm. For irradiation distances of 10–30 mm, disc-shaped dust figures were formed by both charges remaining on the ebonite plate irradiated with an atmospheric-pressure Ar plasma jet. The diameter of the figure decreased with increasing irradiation distance. For an irradiation distance of 2 mm, the dust figures were ring-shaped.

3) Dependence on applied voltage: For a longer irradiation distance (10 mm), no dust figure was observed for applied voltages of 4 or 6 kV but a disc-shaped dust figure was observed for applied voltages of 8 and 10 kV. For a shorter irradiation distance (2 mm), a ring-shaped dust figure was observed for applied voltages of 4–10 kV, and the outer diameter of the ring increased with the applied voltage.

4) Dependence on Ar gas flow rate: When an ebonite plate was irradiated with an atmospheric-pressure Ar plasma jet with an irradiation distance of 10 mm, a disc-shaped dust figure was formed by both charges on the ebonite plate for Ar flow rates of 5 and 10 L/min. The diameter of the disc increased with the Ar gas flow rate.

The differences in the shape and size of the dust figures are due to differences in the spreading pattern of the plasma jet on the ebonite plate. The dust figure method was found to be effective for analyzing the spreading pattern of an atmospheric-pressure plasma jet.

ACKNOWLEDGMENTS

We are grateful to Mr. S. Horie, Mr. T. Tanaka, and Mr. M. Uchino of Photron Limited for their cooperation in the high-speed camera observation.

[1] G. C. Lichtenberg, Novi Comment. Göttingen **8**, 168 (1777).
[2] M. Toepler, Arch. Elektrotech. **10**, 157 (1921).
[3] P. O. Pedersen, Ann. Phys. **374**, 205 (1922).
[4] K. Umeda and M. Syoyama, IEE Japan **50**, 1006 (1930) [in Japanese].
[5] U. Shinohara, IEE Japan **51**, 738 (1931) [in Japanese].
[6] U. Shinohara, IEE Japan **52**, 218 (1932) [in Japanese].

[7] Y. Toriyama and U. Shinohara, Arch. Elektrotech. **28**, 105 (1934).
[8] F. H. Merril and A. von Hipple, J. Appl. Phys. **10**, 873 (1939).
[9] E. Nasser and L. B. Loeb, J. Appl. Phys. **34**, 3340 (1963).
[10] Y. Takahashi, J. Electrostatics **6**, 1 (1979).
[11] Y. Toriyama, *Dust Figures of Surface Discharge and Its Application* (Kinokuniya Press, Tokyo, 1961).
[12] Y. Toriyama, IEE Japan **48**, 523 (1928) [in Japanese].
[13] Y. Toriyama, IEE Japan **48**, 1177 (1928) [in Japanese].
[14] Y. Toriyama, IEE Japan **49**, 393 (1929) [in Japanese].
[15] Y. Toriyama, IEE Japan **49**, 922 (1929) [in Japanese].
[16] Y. Toriyama, IEE Japan **50**, 82 (1930) [in Japanese].
[17] Y. Toriyama, Phys. Rev. **37**, 619 (1931).
[18] Y. Murooka and S. Koyama, J. Appl. Phys. **44**, 1576 (1973).
[19] N. Ando and F. Numajiri, IEEE Trans. Electr. Insul. EI-**14**, 36 (1979).
[20] Y. Manabe, T. Shimazaki, I. Tsuneyasu, and M. Hara, T. IEE Japan 114-A, 710 (1994) [in Japanese].
[21] H. Kuwahata and R. Ohyama, Hyomen Kagaku **30**, 174 (2009) [in Japanese].
[22] H. Kuwahata, T. Haraki, and I. Mikami, e-J. Surf. Sci. Nanotech. **11**, 36 (2013).
[23] H. Kuwahata and T. Yamaguchi, e-J. Surf. Sci. Nanotech. **14**, 231 (2016).
[24] H. Kuwahata, T. Yamaguchi, R. Ohyama, and A. Ito, Jpn. J. Appl. Phys. **54**, 01AG08 (2015).
[25] H. Kuwahata, T. Yamaguchi, H. Kojima, and K. Kabayama, Hyomen Kagaku **36**, 257 (2015) [in Japanese].
[26] H. Kuwahata, K. Kimura, and R. Ohyama, e-J. Surf. Sci. Nanotech. **8**, 381 (2010).
[27] R. Ohyama and A. Nagai, Japan Patent, 244938 (2006).
[28] H. Kuwahata and T. Yamaguchi, e-J. Surf. Sci. Nanotech. **13**, 474 (2015).
[29] Y. Murooka and Y. Toriyama, Br. J. Appl. Phys. **18**, 1607 (1967).